Atomistic simulation of the mechanical response of a nanoporous body-centered cubic metal

C.J. Ruestes,[a,*] E.M. Bringa,[a,b] A. Stukowski,[c] J.F. Rodríguez Nieva,[d] G. Bertolino,[e] Y. Tang[f] and M.A. Meyers[f]

[a]*Instituto de Ciencias Básicas, Univ. Nac. de Cuyo, Mendoza 5500, Argentina*
[b]*CONICET, Mendoza 5500, Argentina*
[c]*Lawrence Livermore National Laboratory, Livermore, CA 94550, USA*
[d]*Massachusetts Institute of Technology, MA 02139, USA*
[e]*CONICET - Centro Atómico Bariloche, Bariloche 8400, Argentina*
[f]*University of California, San Diego, La Jolla, CA 92093, USA*

Uniaxial strain compression of a Ta monocrystal containing randomly placed nanovoids was studied using molecular dynamics simulations. Interacting voids decrease the stress required for the onset of plasticity, in comparison with earlier studies for isolated voids. Dislocations resulting from loading are emitted from void surfaces as shear loops, with their interactions leading to hardening. Plastic activity leads to a decrease in porosity, with voids disappearing at 14% strain. The resulting dislocation densities agree well with experimental results.
© 2013 Acta Materialia Inc. Published by Elsevier Ltd. All rights reserved.

Materials with nanoporosity have unique characteristics that render them potentially attractive for advanced applications, for instance requiring exceptional mechanical properties [1] or radiation resistance [2]. Nanoporosity can arise from mechanical failure, as in incipient spall [3], from radiation damage [4] or as a result of their fabrication process itself, as in powder sintering or dealloying [1].

Understanding the mechanical deformation of such nanofoams should help in the design of materials with improved mechanical properties. Mechanical deformation of such nanofoams under extreme conditions is not well understood because experiments that probe pressure-induced nanovoid collapse at the relevant nanoscopic length and ultrashort time scales are extremely difficult with current set-ups, while continuum models might not work at the nanoscale. In recent years, laser-driven shock waves with strain rates of $10^7 - 10^9 \, s^{-1}$ have been used to investigate the dynamic behavior of a number of bulk materials [5–10], including body-centered cubic (bcc) metals like tantalum [5], vanadium [7] and iron [10]. The use of atomistic molecular dynamics (MD) simulations in conjunction with these experiments has led to the elucidation of important mechanisms of plastic deformation operating in these regimes [9], and to the creation of new constitutive models [11,12].

Here we extend our previous MD simulations of the collapse of a single nanovoid in both face-centered cubic [13,14] and bcc [15,16] metals to the collapse of a collection of nanovoids in a bulk bcc Ta sample. There are several atomistic studies of single void collapse at high strain rates [17–19], including a quasi-continuum study [20], but relatively few studies for a collection of voids [21–23]. This work focuses on dislocation activity and the resulting stress relaxation, which has not been discussed in depth in the studies mentioned above.

The molecular dynamics code LAMMPS [24] was used in this study to perform deformation simulations with the extended Finnis–Sinclair potential for Ta by Dai et al. [25]. This potential gives the correct volume–pressure relation up to pressures of few hundred gigapascals [25] according to static equilibrium simulations.

* Corresponding author. Tel.: +1 8589008425; e-mail: cjruestes@hotmail.com

However, non-equilibrium shock simulations, where defects or new phases can nucleate, impose additional demands on empirical potentials [26–29]. We tested the potential by Dai et al. [25] up to 60 GPa, since our simulations did not go beyond 50 GPa. We did not find any signature of artificial behavior, like soft-phonon modes [27] or solid–solid phase transitions [29].

The cubic simulation domain contained a tantalum single crystal of $100 \times 100 \times 100$ unit cells, with 10 randomly distributed spherical voids of $\sim$3.3 nm radius, having an average distance between centers of $\sim$17 nm. This corresponds to a void volume fraction of 4.1%. Periodic boundary conditions were applied in all directions. The domain was subjected to uniaxial compressive strain along the [0 0 1] direction, with zero lateral strain to mimic shock experiments [5–10]. The simulation was conducted at a strain rate of $10^9 \, \mathrm{s}^{-1}$ (200 ps, 20% volumetric strain) and at an initial temperature of 300 K. The sample was equilibrated to reach zero pressure and the prescribed initial temperature prior to the application of the uniaxial strain. In order to capture temperature effects related to plasticity, no temperature control was used during loading. Identification of defects was done using the common neighbor analysis method [30,31] and the dislocation extraction algorithm (DXA) [32]. The latter enables one to identify line and surface defects and to measure dislocation densities. Visualization of the defects was performed using ParaView [33].

The von Mises stress is shown in Figure 1a, with the temperature evolution shown in Figure 1b. The stress in the loading direction, σ_{ZZ}, can be compared to values by Tang et al. [15] for a cube of the same dimensions with a single void of 3.3 nm radius in the center of the simulation cell. This stress is lower in the sample with 10 voids than in the single void sample ($\sigma_{1v}/\sigma_{10v} \sim 1.2$). This decrease in the stress for the onset of plasticity is due to the interaction between voids: at the same remote applied stress, the local stresses are different due to the overlap and additive nature of the strain fields.

The evolution of the von Mises stress–strain response begins with an elastic stage, up to a strain of 0.055. As the stress resulting from the applied strain increases, dislocations begin to nucleate on the atomic steps found on the void surfaces, often referred as ledges [13], and start moving. This marks the onset of plasticity, as shown with an arrow in Figure 1a. There is an associated temperature increase due to the dissipative nature of dislocation motion, shown in Figure 1b.

Once the maximum flow stress is reached, a plateau is seen in the stress–strain curve prior to an incipient relaxation up to a strain of 0.14. Upon subsequent straining, the flow stress begins to increase again. The onset of strain hardening coincides with the collapse of voids, as shown below. Dislocations evolve rapidly following nucleation, as shown in Figure 2. Plastic deformation proceeds through the emission of perfect dislocation shear loops from void surfaces, with loop extremities terminating at void surfaces in a mechanism which has been already discussed by Bringa et al. [14] and Tang et al. [15]. The dislocation loops are the same as the ones identified by Rudd [17] and Tang et al. [15]. The loop planes are $\{0\bar{1}1\}$ and the Burgers vectors of the dislocations are $1/2 <111>$.

The edge components of the dislocations have a higher mobility and advance rapidly, leaving behind straight screw dislocation segments. At a strain of 0.07, loops form junctions with dislocations emitted from adjacent voids, generating a complex dislocation forest. The collapse of the voids progresses with the continued emission, propagation and interaction of dislocations (strains of 0.075–0.10).

Several experimental studies show the presence of twins in Ta samples deformed at high strain rates
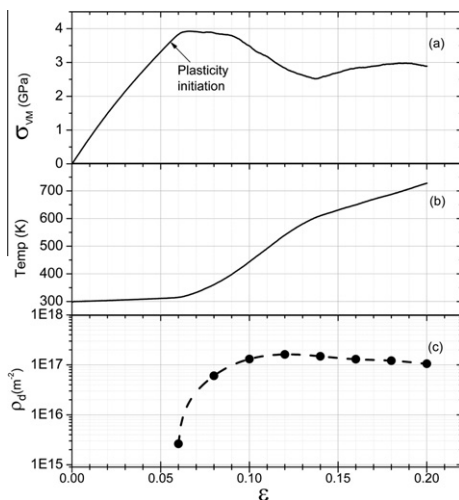
Figure 1. (a) von Mises stress–strain curve. The strain at which defects start nucleating is indicated by an arrow. Strain hardening is noticeable at strains larger than 0.14, consistent with the complete collapse of the voids. (b) Temperature evolution shows the effect of plasticity on the global heating of the sample. The slope changes significantly when plasticity begins. (c) Dislocation density measured using the DXA.
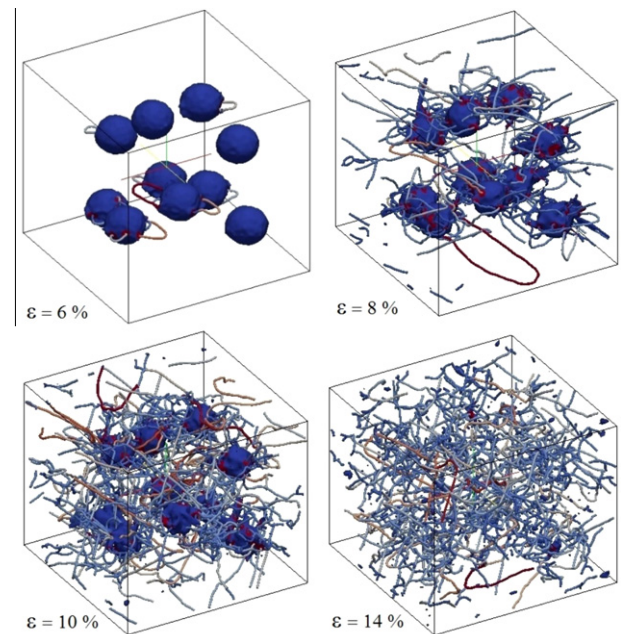
Figure 2. Development of the dislocation forest. A 2% strain increment corresponds to 20 ps of time evolution. Note the long screw segments, also seen in experimentally recovered samples. No porosity is seen at 14% strain, as discussed in the text.

[3,34]. However, we cannot find evidence of twinning in the current simulations. This is probably due to the high density of dislocation sources provided by void surfaces, which relax the deviatoric stresses and inhibit plastic deformation by twins.

We measured dislocation densities using the DXA [32]. The densities obtained with the DXA are not affected by the presence of non-dislocation defects, which are effectively eliminated by means of a Burgers circuit test. Figure 1c shows the measured dislocation density. Once plasticity starts, the total dislocation density rapidly reaches values consistent with those of highly work-hardened metals (10^{15}–10^{17} m^{-2}).
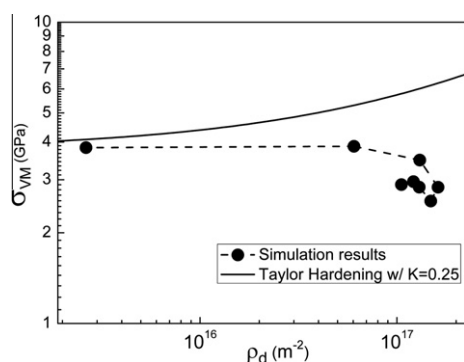
Nemat-Nasser et al. [35] obtained dislocation densities up to 10^{17} m^{-2} for polycrystalline Ta experimental tests at a strain rate above 5×10^4 s^{-1}. Hsiung [34] recently achieved dislocation densities above 10^{16} m^{-2} for pure Ta explosively shocked at peak pressures of 30 GPa.

The strain hardening of tantalum has been studied with quasi-static experiments [36] and simulations of nanocrystals (nc) [37]. Both works report the achieved hardening effect in terms of the shear modulus, G. The shear modulus taken for our characterization is 87.4 GPa, corresponding to the C_{44} value reported in Ref. [25] for the extended Finnis–Sinclair potential. For our simulations, two regions were identified; the first was for strain values from 0.14 to 0.155, with a hardening slope of 0.18G. The second region of strain hardening corresponds to strain values from 0.16 to 0.185, with a lower hardening, 0.06G. The factor 40 difference between our high-strain-rate simulations and the quasi-static experiments [36] can be explained by the strain rate effects. The factor of 4 between our single crystal and the nc simulations [37] is likely due to additional grain boundary relaxation processes in the nc sample.

In an attempt to characterize the strain hardening behavior of the sample, the von Mises stress is related to the calculated dislocation density in Figure 3, where we also include the dependence predicted by a simple Taylor hardening model [38]:

$$\sigma = \sigma_0 + K \cdot G \cdot b \cdot \rho_d^{1/2} \qquad (1)$$
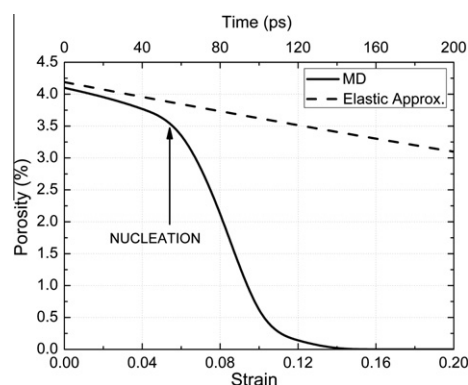
with K a constant typically taken as 0.25 for dislocation densities around 10^{16} m^{-2} [39]. A term accounting for frictional stress acting on an isolated dislocation, σ_0, is routinely added to the original Taylor equation. This term is taken, as a first approximation, as the Peierls–Nabarro stress for Ta, with a calculated value of 3.76 GPa [40]. It can be seen that the Taylor stress is somewhat lower in our simulations. The degree of work hardening is higher for the Taylor prediction. In the Taylor approach, the geometrically necessary dislocation emission is not incorporated and the dislocation density is an arbitrary function of strain. Taylor hardening comes from interaction among dislocations, but in the current simulations the stress level is also determined by emission of dislocation loops from voids. We have a softening mechanism: new dislocation generation from void surfaces and their motion, which relaxes the shear stress stress. The initial porosity of the sample was 4.1% and its evolution is plotted in Figure 4, together with a purely elastic approximation. Up to 6% strain (60 ps), the porosity decreases with a slope slightly larger than the one corresponding to the elastic approximation. In the range from 6 to 10% strain, the porosity suffers a steep decrease in a short time frame (40 ps), consistent with dislocation-mediated void collapse [41]. In agreement with Tang et al. [15] and Marian et al. [20], loops remain attached to void surfaces during uniaxial compression [14]. Voids collapse completely at a strain of 14% (140 ps); at this point, the strain hardening effect becomes noticeable in the stress–strain plot (Fig. 1a).

In summary, this study has demonstrated that nanovoid configurations lead to an elastoplastic response that is significantly different from that of a monocrystal by virtue of the generation of shear dislocation loops, which propagate and interact. The methodology of this study could lead to an understanding of the mechanical response of nanofoams, which have a significant potential for use by virtue of the nanoscale effects [1,2]. MD simulations show that plastic deformation proceeds by the emission of dislocation loops from ledges present on the void surfaces, and by their propagation and interaction as they encounter loops from adjacent voids. The dislocation density rises rapidly as voids start to shrink. The strain level at which defects start to nucleate is about 80% of the value reported by Tang et al. [15] for a single void in Ta subject to uniaxial compression, due to void–void interactions. Total dislocation densities are

Figure 3. von Mises stress as function of the total dislocation density, compared with a Taylor hardening model with $K = 0.25$ [39] and an initial stress equal to the Peierls–Nabarro stress [40].

Figure 4. Porosity evolution during compression as a function of time and strain.

10^{16}–10^{17} m^{-2}, in agreement with experimental results for deformation of Ta at high strain rate [36,37]. No twinning was observed, in agreement with simulations of uniaxial compression of single voids in Ta [15]. The behavior of the von Mises stress related to the total dislocation density observed above 0.14 strain is lower than predicted by a simple Taylor hardening model or in conventional tensile or compressive tests. This is a consequence of the multiple dislocation sources provided by the voids, which decrease the necessity for multiplication and rapid density increase in plastic deformation of bulk (void-free) monocrystals, and of the shrinking of voids with a reduction of the overall volume.

[1] J. Biener, A.M. Hodge, J.R. Hayes, C.A. Volkert, L.A. Zepeda-Ruiz, A.V. Hamza, F.F. Abraham, Nano Lett. 6 (2006) 2379.
[2] E.M. Bringa, J.D. Monk, A. Caro, A. Misra, L. Zepeda-Ruiz, M. Duchaineau, F. Abraham, M. Nastasi, S.T. Picraux, Y.Q. Wang, D. Farkas, Nano Lett. 12 (2012) 3351.
[3] G.T. Gray III, A.D. Rollett, in: R. Asfahani, E. Chen, A. Crowson (Eds.), High Strain Rate Behavior of Refractory Metals and Alloys, TMS, Warrendale, PA, 1992, pp. 303–315.
[4] R.M. Mayer, L.M. Brown, J. Nucl. Mater. 1–2 (1980) 46.
[5] C.H. Lu, B.A. Remington, B.R. Maddox, B. Kad, H.S. Park, S.T. Prisbrey, M.A. Meyers, Acta Mater. 60 (2012) 6601.
[6] E. Loomis, D. Swift, J. McNaney, H. Lorenzana, P. Peralta, Acta Mater. 56 (2008) 3647.
[7] D.H. Kalantar, G.W. Collins, J.D. Colvin, J.H. Eggert, J. Hawreliak, H.E. Lorenzana, M.A. Meyers, R.W. Minich, K. Rosolankova, M.S. Schneider, J.S. Stolken, J.S. Wark, Int. J. Impact Eng. 33 (2006) 343.
[8] H.N. Jarmakani, E.M. Bringa, P. Erhart, B.A. Remington, Y.M. Wang, N.Q. Vo, M.A. Meyers, Acta Mater. 56 (2008) 5584.
[9] B. Cao, E.M. Bringa, M.A. Meyers, Metall. Mater. Trans. A 38 (2007) 2681.
[10] B. Yaakobi, T.R. Boehly, D.D. Meyerhofer, T.J.B. Collins, B.A. Remington, P.G. Allen, S.M. Pollaine, H.E. Lorenzana, J.H. Eggert, Phys. Rev. Lett. 95 (2005) 075501.
[11] N.R. Barton, J.V. Bernier, R. Becker, A. Arsenlis, R. Cavallo, J. Marian, M. Rhee, H.-S. Park, B.A. Remington, R.T. Olson, J. Appl. Phys. 109 (2011) 073501.
[12] R.A. Lebensohn, E.M. Bringa, A. Caro, Acta Mater. 55 (2007) 261.
[13] E.M. Bringa, S. Traiviratana, M.A. Meyers, Acta Mater. 58 (2010) 4458–4477.
[14] E.M. Bringa, V.A. Lubarda, M.A. Meyers, Scr. Mater. 63 (2010) 148.
[15] Y. Tang, E.M. Bringa, B.A. Remington, M.A. Meyers, Acta Mater. 59 (2011) 1354.
[16] Y. Tang, E.M. Bringa, M.A. Meyers, Acta Mater. 60 (2012) 4856.
[17] R.E. Rudd, Philos. Mag. 89 (2009) 3133.
[18] L.P. Dávila, P. Erhart, E.M. Bringa, M.A. Meyers, V.A. Lubarda, M.S. Schneider, R. Becker, M. Kumar, Appl. Phys. Lett. 86 (2005) 161902.
[19] T. Hatano, Phys. Rev. Lett. 92 (2004) 015503.
[20] J. Marian, J. Knap, M. Ortiz, Acta Mater. 53 (2005) 2893.
[21] E.T. Seppälä, J.F. Belak, R.E. Rudd, Phys. Rev. B 71 (2005) 064112.
[22] P. Erhart, E.M. Bringa, M. Kumar, K. Albe, Phys. Rev. B 72 (2005) 052104.
[23] T.C. Germann, K. Kadau, P.S. Lomdahl, in: Proceedings of IEEE/ACM Supercomputing, 2005.
[24] S.J. Plimpton, J. Comp. Phys. (1995) 117.
[25] X.D. Dai, Y. Kong, J.H. Li, B.X. Liu, J. Phys.: Condens. Matter. 18 (2006) 4527.
[26] E.M. Bringa, J.U. Cazamias, P. Erhart, J. Stölken, N. Tanushev, B.D. Wirth, R.E. Rudd, M.J. Caturla, J. Appl. Phys. 96 (2004) 3793.
[27] G. Kimminau, P. Erhart, E.M. Bringa, B. Remington, J.S. Wark, Phys. Rev. B 81 (2010) 092102.
[28] R.F. Zhang, J. Wang, I.J. Beyerlein, T.C. Germann, Philos. Mag. Lett. 91 (2011) 731.
[29] R. Ravelo, Q. An, T.C. Germann, B.L. Holian, AIP Conf. Proc. 1426 (2012) 1263.
[30] D. Faken, H. Jónsson, Comput. Mater. Sci. 2 (1994) 279.
[31] H. Tsuzuki, P.S. Branicio, J.P. Rino, Comput. Phys. Comm. 177 (2007) 518.
[32] A. Stukowski, K. Albe, Model. Simul. Mater. Sci. Eng. 18 (2010) 085001.
[33] A. Henderson, ParaView Guide, A Parallel Visualization Application. Kitware Inc., 2007.
[34] L.L. Hsiung, J. Phys.: Condens. Matter. 22 (2010) 385702.
[35] S. Nemat-Nasser, J.B. Isaacs, M. Liu, Acta Mater. 46 (1998) 1307.
[36] T.E. Mitchell, W.A. Spitzig, Acta Metall. 13 (1965) 116979.
[37] R.E. Rudd, Mater. Sci. Forum 633–634 (2010) 3.
[38] G.I. Taylor, Proc. R. Soc. London, A 145 (1934) 362.
[39] L.M. Brown, Mater. Sci. Technol. Ser. 28 (2012) 1209.
[40] R. Gröger, V. Vitek, Philos. Mag. 89 (2009) 3163.
[41] S. Traiviratana, E.M. Bringa, D.H. Benson, M.A. Meyers, Acta Mater. 56 (2008) 3874.